BIOCHEMISTRY
including biophysical chemistry & molecular biology
Article

Biochemistry **2011,** *50,* 1091–1100 1091
DOI: 10.1021/bi101741v

Toxoflavin Lyase Requires a Novel 1-His-2-Carboxylate Facial Triad[†,‡]

Michael K. Fenwick,[§] Benjamin Philmus,[∥] Tadhg P. Begley,*[,∥] and Steven E. Ealick*[,§]

[§]*Department of Chemistry and Chemical Biology, Cornell University, Ithaca, New York 14853, United States, and* [∥]*Department of Chemistry, Texas A&M University, College Station, Texas 77843, United States*

Received October 29, 2010; Revised Manuscript Received December 17, 2010

ABSTRACT: High-resolution crystal structures are reported for apo, holo, and substrate-bound forms of a toxoflavin-degrading metalloenzyme (TflA). In addition, the degradation reaction is shown to be dependent on oxygen, Mn(II), and dithiothreitol in vitro. Despite its low sequence identity with proteins of known structure, TflA is structurally homologous to proteins of the vicinal oxygen chelate superfamily. Like other metalloenzymes in this superfamily, the TflA fold contains four modules that associate to form a metal binding site; however, the fold displays a rare rearrangement of the structural modules indicative of domain permutation. Moreover, unlike the 2-His-1-carboxylate facial triad commonly utilized by vicinal oxygen chelate dioxygenases and other dioxygen-activating non-heme Fe(II) enzymes, the metal center in TflA consists of a 1-His-2-carboxylate facial triad. The substrate-bound complex shows square-pyramidal geometry in which one position is occupied by O5 of toxoflavin. The open coordination site is predicted to be the dioxygen binding site. TflA appears to stabilize the reduced form of toxoflavin through second-sphere interactions. This anionic species is predicted to be the electron source responsible for reductive activation of oxygen to produce a peroxytoxoflavin intermediate.

Toxoflavin (Figure 1A) is an azapteridine that is toxic to various plants, fungi, animals, and bacteria. It is synthesized by several bacteria, including *Burkholderia glumae*, *Burkholderia plantarii*, *Burkholderia gladioli* pathovar *cocovenenans*, and *Streptomyces* (*1*, *2*). Toxoflavin toxicity is attributed to its ability to act as an effective electron carrier, which allows it to bypass the cytochrome electron transport system and produce hydrogen peroxide in the presence of oxygen (*3*, *4*).

Recently, toxoflavin has attracted growing interest, particularly in the agricultural sciences. Infection of rice plants by toxoflavin-producing bacteria has led to significant losses of rice crops in the United States and Asia (*5*−*8*). The identification of toxoflavin as the virulent agent motivated the development of transgenic plants that degrade toxoflavin by expressing the toxoflavin lyase gene (*tflA*) of *Paenibacillus polymyxa* JH2 (*9*). Unlike their nontransgenic counterparts, these plants were found to grow normally when treated with toxoflavin. In vitro, the enzymatic degradation of toxoflavin by TflA was shown to depend on Mn(II) and the reducing agent dithiothreitol (DTT)[1] (*9*); however, neither the molecular mechanism underlying the reaction nor the reaction product is known.

Here, we report crystal structures of metal free TflA (apo), Mn(II)-bound TflA (holo), and the holo-TflA−toxoflavin complex. In addition, we demonstrate biochemically that the conversion of toxoflavin requires molecular oxygen in addition to Mn(II) and a reducing agent (*9*). The crystal structures show that TflA adopts a structural fold similar to that of vicinal oxygen chelate (VOC) superfamily proteins (*10*−*13*) and contains a Mn(II) site. One of the key distinguishing features of TflA is its utilization of a 1-His-2-carboxylate facial triad of Mn(II)-binding ligands characterized by one histidine residue and two monodentate carboxylate groups, similar to the 2-His-1-carboxylate facial triad (*14*). In the toxoflavin complex, the Mn(II) is also chelated by O5 from toxoflavin and a water molecule, with the open coordination site being the putative dioxygen binding site. Second-sphere interactions provide clues about the tautomeric state and charge of the bound toxoflavin. From this structure and the dependence of the reaction on a reducing agent, a molecular model of a peroxytoxoflavin intermediate was constructed.

MATERIALS AND METHODS

Protein Expression and Purification. The toxoflavin lyase analyzed in this study comprised the 221-residue product of the *tflA* gene from *P. polymyxa* JH2 (*9*) and the N- and C-terminal polyhistidine tags MGSDKIHHHHHHSSGENLYFQGH and LEHHHHHH, respectively. The native protein was expressed in *Escherichia coli* BL21(DE3) grown in Luria-Bertani medium. Typically, cells were grown in baffled shaker flasks at 37 °C until an OD_{600} of 0.5−0.9 was reached. The flasks were then moved to

[†]This work was supported by the Robert A. Welch Foundation (A-0034 to TPB) and National Institutes of Health Grant GM73220 (S.E.E.) and is based upon research conducted at the Advanced Photon Source on the Northeastern Collaborative Access Team beamlines, which are supported by Grant RR-15301 from the National Institutes of Health, and at the Cornell High Energy Synchrotron Source (CHESS), which is supported by Grant RR-01646 from the National Institutes of Health. Use of the Advanced Photon Source is supported by the U.S. Department of Energy, Office of Basic Energy Sciences, under Contract DE-AC02-06CH11357. CHESS is supported by the National Science Foundation (Grant DMR-0225180) and the National Institute of General Medical Sciences.

[‡]The coordinates of apo, holo, and toxoflavin-bound TflA have been deposited as Protein Data Bank entries 3PKV, 3PKW, and 3PKX, respectively.

*To whom correspondence should be addressed. S.E.E.: Department of Chemistry and Chemical Biology, Cornell University, Ithaca, NY 14853; telephone, (607) 255-7961; fax, (607) 255-1227; e-mail, see3@cornell.edu. T.P.B.: e-mail, begley@chem.tamu.edu.

[1]Abbreviations: TflA, toxoflavin lyase; DTT, dithiothreitol; VOC, vicinal oxygen chelate; SeMet, selenomethionine; PDB, Protein Data Bank; PEG, polyethylene glycol; SAD, single-wavelength anomalous dispersion; CAPS, 3-(cyclohexylamino)-1-propanesulfonic acid; rmsd, root-mean-square deviation; DHBD, 2,3-dihydroxybiphenyl 1,2-dioxygenase; HPPD, 4-hydroxyphenylpyruvate dioxygenase; MWCO, molecular weight cutoff.

© 2010 American Chemical Society
Published on Web 12/17/2010

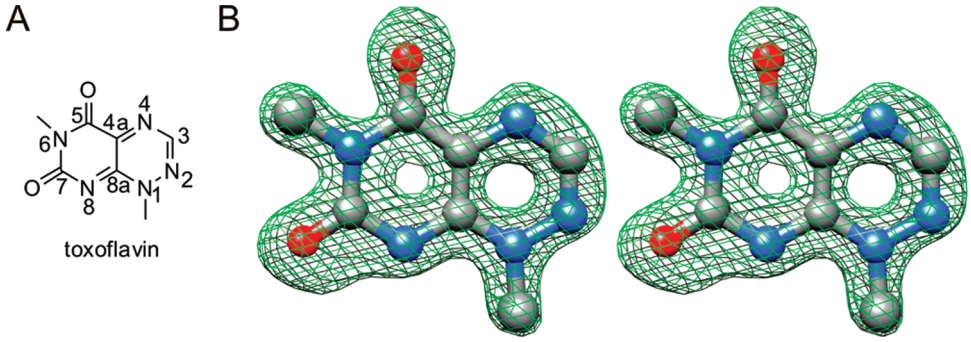

FIGURE 1: Structure of toxoflavin. (A) Structural formula and numbering for toxoflavin. (B) $F_o - F_c$ electron density map for toxoflavin. The map is contoured at 3σ. The map was generated using the structure factors for the complex and the refined model of the complex with toxoflavin omitted.

ice for approximately 1 h, supplemented with isopropyl 1-β-D-galactopyranoside (0.5 mM), and shaken again at 15 °C for a minimum of 18 h. Cell pellets from 1 or 2 L of culture were lysed via sonication on ice and centrifuged twice at 4 °C and 55000*g* for at least 25 min per cycle. The resulting supernatants were subjected to nickel-affinity chromatography, and the purity of the protein was verified to be in excess of 95% by sodium dodecyl sulfate−polyacrylamide gel electrophoresis analysis (*15*). Selenomethionine-substituted TflA (SeMet-TflA) was expressed in *E. coli* B834 grown in 4 L of M9 minimal medium containing 4 g/L dextrose, 50 mg/L L-SeMet, the 19 remaining L-amino acids (at 40 mg/L), 2 mM $MgSO_4$, 0.1 mM $CaCl_2$, 25 mg/L $FeSO_4$, a 1× minimal essential medium vitamin solution (Invitrogen), and 40 mg/L kanamycin. These cells were grown and induced as described for the BL21 cultures. SeMet-TflA was purified by nickel-affinity and size exclusion chromatography using buffers supplemented with 1−2 mM DTT. Purified TflA was concentrated to approximately 50 mg/mL on the basis of measurements of light absorbance at 280 nm and an estimated extinction coefficient of 23000 M^{-1} cm^{-1} (*16*).

Crystallization and Structure Determination. Crystals were grown using hanging drop vapor diffusion starting with a 1:1 protein:reservoir solution ratio and equilibrated at 22 °C. For crystallization of the native protein, the reservoir solution consisted of 1.2 M NaH_2PO_4, 0.8 M K_2HPO_4, 0.1 M 3-(cyclohexylamino)-1-propanesulfonic acid (CAPS) (pH 10.5), and 0.2 M Li_2SO_4. Crystals of SeMet-TflA grew in drops made from a modified reservoir solution of 1.05 M NaH_2PO_4, 0.86 M K_2HPO_4, 0.091 M CAPS (pH 10.5), 0.14 M Li_2SO_4, and 18 mM DTT.

Prior to cryo-cooling, the crystals of apo-TflA were soaked in a cryoprotectant consisting of a 1:1 ratio of reservoir buffer and a solution of 30% (v/v) glycerol and 30% (v/v) ethylene glycol to which $MnCl_2$ was added to a final concentration of 5 mM; however, no density for Mn(II) was observed in the active site for this particular structure. For the TflA−Mn(II)−toxoflavin complex, crystals were first transferred into drops of stabilizing solution prepared from 3 μL of 25% (w/v) PEG3000 and 1% (v/v) reservoir solution, where 0.2 M Li_2SO_4 was replaced with 0.2 M NaCl (final pH of 6.4), 0.5 μL of 25 mM $MnCl_2$, and 0.5 μL of 2.5 mM toxoflavin. The toxoflavin concentration was then increased through two 0.5 μL additions of 10 and 100 mM stocks, after which the crystals were allowed to soak for approximately 45 min. Immediately preceding cryo-cooling, 2 μL of 0.2 M DTT followed by 3 μL of 50% (w/v) PEG3000 was added to these drops, and the crystals were picked up and flash-cooled without delay. For the holo-TflA structure, a similar procedure was followed but with toxoflavin replaced by the uncharacterized reaction products; however, in the structure, electron density was present for only Mn(II) and coordinating waters.

Data Collection and Processing. X-ray diffraction experiments were performed at the Advanced Photon Source (APS) and the Cornell High Energy Synchrotron Source (CHESS). In all cases, the rotation method was employed with an oscillation range of 1.0° per frame, and crystals were irradiated at cryogenic temperatures near 100 K. At the APS, the native and SeMet-TflA crystals were exposed to X-rays at the selenium edge for 1.0 s. Images were recorded on an ADSC Q315 CCD detector with a crystal to detector distance of 200 mm. At CHESS, the holo and substrate-bound TflA crystals were exposed to X-rays for 1.5 s. Images were collected using an ADSC Q270 CCD detector with crystal to detector distances of 210 and 190 mm, respectively.

Images were indexed, integrated, scaled, and merged using HKL2000 (*17*). Final sets of merged intensities for the apo, holo, and toxoflavin-bound TflA were derived from 150, 130, and 220 X-ray images and corresponded to 1.34, 1.80, and 1.50 Å resolution, respectively. The final SeMet-TflA data set with unmerged Bijvoet pairs was obtained from 150 images and had a resolution of 1.70 Å. Data collection and processing statistics are summarized in Table 1.

Structure Determination and Refinement. The crystal structure of TflA was determined using single-wavelength anomalous diffraction (SAD) phasing and SeMet-TflA. This crystal belonged to rhombohedral space group *R*3 and had the following unit cell dimensions: a = 110.9 Å, and c = 58.3 Å. The asymmetric unit contained a single copy of the protein, and the estimated solvent content of the unit cell was 49.6%. The selenium substructure corresponding to Met17, Met24, and Met203 was obtained using SHELXD (*18*, *19*). The AutoSol routine of PHENIX (*20*) successfully placed residues 2−221 of SeMet-TflA and Leu222 from the C-terminal tag using the resulting 1.70 Å resolution electron density map. Refinement was conducted using PHENIX, and graphical manipulations were performed with COOT (*21*). The final structural model was refined to R_{work} and R_{free} values of 17.4 and 19.4%, respectively. Refinement statistics are listed in Table 2.

The SeMet-TflA structure was used to provide initial phases for the structures of the apo, holo, and substrate-bound forms of TflA. All crystals belonged to the same space group and had unit cell dimensions similar to those of the SeMet-TflA crystal. Structure refinements were conducted in two steps. The first consisted of seven cycles of maximum likelihood refinement using PHENIX in which water molecules and side chain rotamers were added or updated automatically, and simulated annealing was

Table 1: X-ray Data Collection Statistics

	SeMet-TflA	apo TflA	holo TflA	TflA−toxoflavin−Mn
beamline	APS 24-ID-C	APS 24-ID-C	CHESS F1	CHESS F1
wavelength (Å)	0.9792	0.9792	0.9177	0.9177
space group	*R*3	*R*3	*R*3	*R*3
a (Å)	110.9	110.6	110.9	111.2
c (Å)	58.3	58.1	55.7	57.1
resolution, highest shell (Å)	1.76−1.70	1.39−1.34	1.86−1.80	1.55−1.50
no. of reflections used	136728	269001	92848	278660
no. of unique reflections	58443, 29111[a]	59565	23624	41996
redundancy	4.7 (4.6)[b]	4.5 (3.8)[b]	3.9 (3.7)[b]	6.6 (5.9)[b]
completeness (%)	99.9 (100.0)[b]	99.9 (99.9)[b]	99.6 (100.0)[b]	99.6 (100.0)[b]
$\langle I\rangle/\langle\sigma_I\rangle$[c]	19.6 (3.2)[b]	29.2 (2.9)[b]	17.3 (2.0)[b]	24.7 (1.7)[b]
R_{merge} (%)[d]	7.0 (41.7)[b]	4.3 (41.6)[b]	5.4 (37.1)[b]	5.3 (53.1)[b]

[a]Number of Bijvoet pairs. [b]Values in parentheses are those for the highest-resolution shell. [c]The brackets denote the mean; *I* denotes intensity, and σ_I represents the standard deviation of *I*. [d]$R_{merge} = \sum_{i=1}^{N_U}\sum_{j=1}^{N_i}|I_{ij} - \langle I\rangle_i|/\sum_{i=1}^{N_U}\sum_{j=}^{N_i} I_{ij}$, where N_U is the total number of unique reflections and N_i is the number of reflections measured for a given $i = hkl$.

Table 2: Refinement Statistics

	SeMet-TflA	apo TflA	holo TflA	TflA−toxoflavin−Mn
no. of reflections	28975	57477	22470	38786
no. of reflections in the working set	27529	54657	21350	36893
resolution (Å)	1.70	1.34	1.80	1.50
no. of protein atoms	1733	1772	1725	1733
no. of waters	224	253	147	187
no. of ligand atoms	0	0	0	14
no. of metal ions	0	0	1	1
rmsd from ideal bonds (Å)	0.006	0.006	0.007	0.006
rmsd from ideal angles (deg)	1.067	1.085	1.079	1.032
R_{work} (%)[a]	17.4	17.2	18.9	20.6
R_{free} (%)[a]	19.4	18.5	22.3	23.0
Ramachandran analysis[b]				
most favored (%)	91.3	91.3	89.2	90.2
additional allowed (%)	8.2	8.2	10.3	9.3
generously allowed (%)	0.0	0.0	0.0	0.0
disallowed (%)	0.5	0.5	0.5	0.5

[a]$R_{work} = \sum_{i=1}^{N_U}||F_{o,i}| - k|F_{c,i}||/\sum_{i=1}^{N_U}|F_{o,i}|$, where $|F_{o,i}|$ and $|F_{c,i}|$ are the observed and calculated structure factor amplitudes, respectively, for reflection $i = hkl$ and N_U is the number of unique reflections in the working set. For R_{free}, these sums were taken over a 5% subset of the reflections excluded during structure refinement. [b]Excludes glycine, proline, and end residues.

performed in the first and fourth cycles. Default parameters were employed throughout. The structures were then examined, and modifications to the protein were made where appropriate. For the holo TflA and TflA−Mn(II)−toxoflavin structures, active site water molecules were removed and Mn(II) or toxoflavin and Mn(II) were placed into $F_o - F_c$ electron density (Figure 1B). Toxoflavin was initially built using the electronic ligand builder and optimization workbench in PHENIX (*22*). Beginning with a dihydro form of toxoflavin with atoms N4 and N8 protonated, the AM1 semiempirical quantum mechanical method was employed to obtain ligand coordinates and geometry restraints.

In the second step, five additional rounds of maximum likelihood refinement were performed in PHENIX with water molecule updating. REDUCE (*23*) was applied for choosing side chain orientations for asparagine, glutamine, and histidine residues, and the structure was subsequently analyzed using COOT and PROCHECK (*24*). Finally, water molecules with *B* factors greater than 50.0 Å^2 and a $2F_o - F_c$ map σ level of < 1.0 electron/Å^3 were removed, and all remaining waters were examined individually. Superimposition of native and SeMet-TflA main chain atoms of the apoenzyme showed a root-mean-square deviation (rmsd) of 0.12 Å, indicating that no significant backbone structural changes arose from selenium substitution of the methionyl sulfur atoms.

Molecular Modeling of Peroxytoxoflavin. A molecular model of a peroxytoxoflavin intermediate was constructed on the basis of an assumed reaction of molecular oxygen with C4a of reduced toxoflavin. The model was initially built with an -O-O-H moiety covalently bonded to C4a of toxoflavin. The three-dimensional structure was drawn using ChemSketch (ACD Laboratories) and then optimized in vacuo using the AM1 semiempirical quantum mechanical method within the electronic ligand builder and optimization workbench of PHENIX (*22*). The optimized structure was placed into the active site of TflA by superimposition onto the experimental toxoflavin structure in the holo TflA−toxoflavin complex. The terminal hydrogen atom of the -O-O-H moiety was removed, and the coordinates of the terminal oxygen atom were altered to give a best fit to octahedral coordination. This was done by calculating the torsional angle that minimized the sum of squares of deviations of the five oxygen−Mn(II)−ligand angles from ideal octahedral angles, assuming a fixed optimized O−O bond distance of 1.32 Å and C4a−O−O angle of 116°.

Toxoflavin Synthesis. Toxoflavin was synthesized as previously described (*25*).

UV−Vis Spectroscopy. UV−visible spectra were recorded for solutions of toxoflavin containing or lacking DTT. For the former case, toxoflavin, dissolved in 10 mM potassium phosphate buffer (pH 7.0) to a final concentration of 9 mM, was combined with an equal volume of 10 mM DTT dissolved in water. In the absence of DTT, toxoflavin was mixed with an equal volume of water. UV−visible spectra were recorded using a NanoDrop 2000 (ThermoScientific).

Oxygen Dependence of TflA. For testing the oxygen dependence of the TflA reaction, all the components were allowed to gas exchange in a COY anaerobic chamber operating at <1 ppm O_2 for 30−45 min prior to mixing. The aerobic reaction mixtures were removed from the anaerobic chamber and incubated at room temperature for approximately 1 h, which corresponded to the time required for the control reaction mixture lacking TflA to turn yellow (indicative of toxoflavin reoxidation), and the reaction mixtures were heat denatured (95 °C for 5 min) prior to protein removal. The anaerobic reaction mixtures were left in the anaerobic chamber for 1 h and heat denatured (95 °C for 5 min) prior to being exposed to oxygen. The reaction mixtures were then passed through PALL life sciences protein concentrators [10000 molecular weight cutoff (MWCO), 14000*g*, 30 min, and 4 °C]. Samples (20 μL) of the flow-through volumes were analyzed by HPLC as described below.

TflA Activity Assays. Reaction mixtures consisted of 50 μL solutions of 20 mM Tris (pH 6.5), 10 mM $MnCl_2$, 0.5 mM toxoflavin, and 9 μM TflA, and reactions were initiated by the addition of DTT to a final concentration of 10 mM. At the specified time points (1, 5, 10, 15, and 30 min), the reactions were quenched by addition of 100 μL of 10 M urea followed by filtration through PALL protein concentrators (10000 MWCO, 14000*g*, 30 min, 4 °C). A portion of the reaction mixtures (100 μL) was analyzed via HPLC as described below.

TflA Inactivation Studies. Water (145 μL), 5 μL of Tris (1 M, pH 7.0), and 25 μL of TflA (90 μM) were added to a 1.5 mL microcentrifuge tube. Aliquots (35 μL) were then placed in new microcentrifuge tubes. To each was added 2 μL of water or 2 μL of EDTA (20 mM), and the mixtures were incubated for 1 h at room temperature. To each of these mixtures was added 3 μL of $MnCl_2$ (0.1 M) or 3 μL of water followed by 5 μL of toxoflavin (5 mM), and the reaction was initiated by addition of 5 μL of DTT (0.1 M). The mixtures were then incubated for 2 h at 30 °C followed by addition of 200 μL of 10 M urea. The mixtures were incubated at room temperature for 15−20 min and then filtered through PALL protein concentrators (10000 MWCO, 14000*g*, 30 min, 4 °C), and 100 μL samples of the concentrator flow through were analyzed by HPLC as described below.

HPLC Analysis. HPLC analysis was performed using an Agilent 1200 HPLC system equipped with a quaternary pump and autosampler and monitored with a 1200 DAD detector using a Gemini C6-Phenyl column (4.6 mm × 150 mm, 5 μm, 110 Å, Phenomenex) at a flow rate of 1 mL/min. Line A was water, line B 10 mM potassium phosphate (pH 6.8), and line C methanol. For the time course assays, the following gradient program was used. The column was pre-equilibrated in 100% A prior to sample injection. The composition of the mobile phase was changed to 45% A and 55% B over 10 min using a linear gradient followed by a change to 15% A, 30% B, and 55% C over the next 10 min. The mobile phase was held at this composition for 2 min and then recycled to 100% A in 1 min. The column was then equilibrated in 100% A for 7 min prior to the next injection. For all other assays, the following gradient was used. The mobile phase was initially 100% A and was held for 1 min followed by a change to 50% A and 50% C over the next 6 min. The composition was held at 50% A and 50% B for 3 min and then recycled to 100% A in 1 min. The column was then equilibrated in 100% A for 7 min prior to the next injection.

Large-Scale Purification of the Enzymatic Product. A master mix of 495 μL of 50 mM potassium phosphate (pH 6.8), 80 μL of toxoflavin (5 mM), 80 μL of $MnCl_2$ (0.1 M), and 80 μL of TflA (∼200 μM) was mixed in a microcentrifuge tube. The mixture was aliquoted into a total of four tubes containing 190 μL of master mix, to which 10 μL DTT (0.1 M) was added to initiate the reaction. A total of 14 reactions were performed in this manner. The reaction mixtures were incubated at 30 °C for 45 min followed by centrifugation to eliminate the solid precipitate (14000*g*, 15 min, 4 °C) and then filtered through a PALL protein concentrator (10000 MWCO, 14000*g*, 60 min, 4 °C). The product was then purified by HPLC using a SPLC-18DB column (10 mm × 250 mm, 5 μm, Supelco) at a flow rate of 2 mL/min using an Agilent 1100 HPLC system with a quaternary pump and manual injector in which line A was water and line B methanol. The column was pre-equilibrated in 100% A and upon injection of the sample immediately switched to 95% A and 5% B. This composition was held for 2 min and then changed to 35% A and 65% B over the next 18 min using a linear gradient. This composition was held for 5 min, then the mobile phase recycled to 100% A in 1 min, and the column equilibrated in 100% A for 9 min prior to the injection of the next sample. Typical injection volumes were 25−50 μL. The product eluted at approximately 12 min and was collected, and fractions were pooled. The solvent was removed under evaporation at reduced pressure. The residue was redissolved in 450 μL of water and 50 μL of D_2O and analyzed via NMR spectroscopy. The spectra obtained were insufficient to unambiguously assign a structure to the reaction product.

Figure Preparation. Illustrations were prepared using Chimera (*26*, *27*) and ChemDraw (CambridgeSoft).

RESULTS

Structure of TflA. TflA is an α/β protein formed from two domains each containing a seven-stranded mixed β-sheet (Figure 2A). The β-sheet topology of domain 1 is β2↑β3↓β4↑β1↑β12↓β13↑β14↓, whereas that of domain 2 is similar, β6↑β7↓β8↑β5↑β9↓β11↓β10↑ (Figure 2B). Domains 1 and 2 are related by pseudo-2-fold symmetry and are joined by two crossovers: one joining β4 and β5 and the second joining β11 and β12.

Domain 1 consists of two modules, M_1 and M_4. M_1 contains a βαβββ fold formed by β-strands 1−4 with helix α1 linking strands β1 and β2, and module M_4 contains a βββ fold formed by β-strands 12−14. Similarly, domain 2 also comprises two modules, M_2 and M_3. M_2 contains a βαβββ fold formed by β-strands 5−8 with helix α2 linking β-strands 5 and 6, and M_3 contains a βαββ fold formed by β-strands 9−11 with helix α3 joining β-strands 9 and 10. Modules M_1 and M_2 are structurally similar to each other and are related by pseudo-2-fold symmetry. Modules M_3 and M_4 are also related by the same pseudo-2-fold axis.

The mixed β-sheet of domain 2 makes a U-shaped cavity that harbors a metal binding site, whereas that of domain 1 forms a

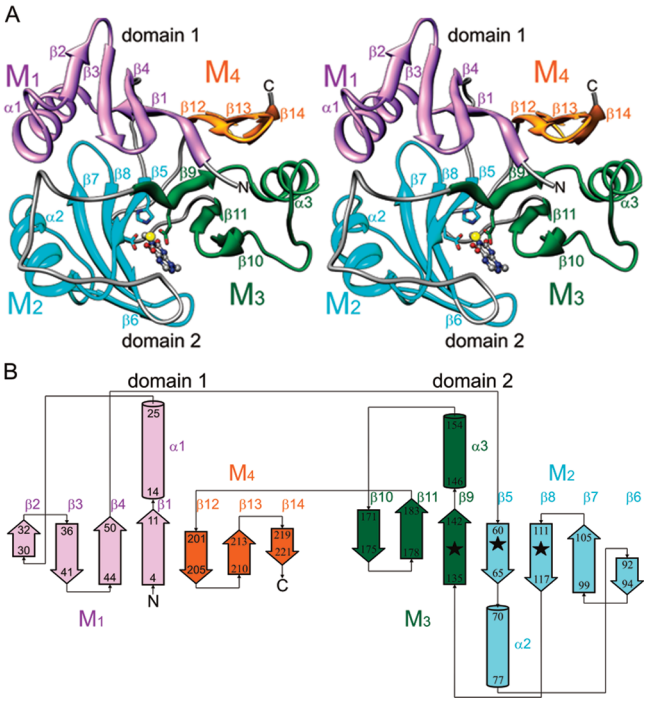

FIGURE 2: Structure of TflA. (A) Ribbon representation of the crystal structure of TflA in a complex with Mn(II) (yellow sphere) and toxoflavin (balls and sticks). The side chains of facial triad residues His60, Glu113, and Glu138 are depicted as sticks, and a metal-chelating water is displayed as a single red sphere. Ribbons and carbon atoms of residues belonging to modules M_1, M_2, M_3, and M_4 are colored purple, cyan, green, and orange, respectively. (B) Secondary structure topology of TflA using the same coloring scheme as in panel A. α-Helices (cylinders) and β-strands (thick arrows) were assigned using DSSP (*54*). The locations of the facial triad residues are marked with black stars.

flatter surface that lacks a metal binding site. The two domains pack together with their β-sheets back to back such that M_1 packs against M_2 and M_3 packs against M_4. The three α-helices are largely solvent-exposed and reside outside the β-sheet core.

TflA Active Site. In the substrate-bound complex, toxoflavin interacts with TflA residues in M_2, M_3, and the loop connecting M_3 and M_4 (Figure 3). O5 of toxoflavin makes a hydrogen bond with the hydroxyl of Tyr103. The triazine ring shows partial π-stacking with the side chain of Phe94. The N1 methyl group and the triazine ring form hydrophobic interactions with Leu170 and Phe172, respectively. The pyrimidine ring forms hydrophobic interactions with the side chains of Leu190 and Trp189 in the loop connecting M_3 and M_4. O7 and N8 of toxoflavin form hydrogen bonds to the guanidinium group of Arg187, and O7 forms a hydrogen bond to the backbone nitrogen atom of Leu190. Complex formation also results in a coordinate covalent bond between O5 of toxoflavin and Mn(II), and hydrogen bonds between N2 of toxoflavin and W4, and between N4 of toxoflavin and W3.

Inferred hydrogen bonds involving N2, N4, and N8 suggest a toxoflavin protonation state compatible with the reduced form, which is required for catalysis. O7 and N8 of toxoflavin accept hydrogen bonds from Arg187, suggesting N8 is not protonated. W3 donates hydrogen bonds to Glu113 and Glu138 (both metal ligands), suggesting that it accepts a hydrogen bond from N4 of toxoflavin (2.9 Å). The local atomic geometry around N2 of toxoflavin is less informative. The N2−W4 distance is 3.1 Å; however, if N2 were protonated, the N2−H···W4 angle would

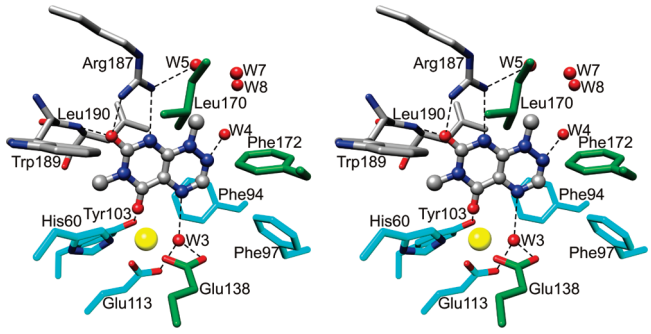

FIGURE 3: Stereodiagram of the TflA active site. Active site side chains of TflA are depicted as sticks with the carbon atoms of residues in M_2, M_3, and the loop connecting M_3 and M_4 colored cyan, green, and gray, respectively. Toxoflavin is shown in ball and stick representation. Mn(II) is represented as a yellow sphere, and waters are shown as red spheres.

be 117°, suggesting that N2 is not likely to act as a strong hydrogen bond donor.

Mn(II) Binding Site. The metal binding site consists of a facial triad comprising residues His60, Glu113, and Glu138 (1-His-2-carboxylate). His60 and Glu113 are located in β5 and β8, respectively, and Glu138 resides in β9. The side chains of these residues extend into the active site cavity to supply three cis ligands for Mn(II), leaving three open coordination sites for other ligands.

In the apoenzyme, Nε2 of His60 forms a hydrogen bond with one of the carboxylate oxygen atoms of Glu138 (Figure 4A). Water molecules W1, W3, and W6 occupy positions opposite the facial triad in the unoccupied Mn(II) binding site. Water molecule W1 hydrogen bonds to the hydroxyl of Tyr103. The electron density for water molecules W3 and W6 is less distinct than that for W1, and the hydrogen bonding interactions are probably dynamic.

In the holoenzyme, the three open coordination sites are occupied by water molecules, which all have well-defined electron density. The overall arrangement of the coordination sphere is octahedral (Figure 4B), with all of the 15 ligand−Mn(II)−ligand angles being within 15° of ideal octahedral angles. None of the water molecule−Mn(II) distances suggest hydroxide character. Rather, all of the water molecules (W1, W2, and W3) are separated from Mn(II) by at least 2.2 Å, which is consistent with overall neutrality for the metal center. Water molecules W1 and W3 form hydrogen bonds with second-sphere water molecules and protein ligands. W1 forms a hydrogen bond to the hydroxyl of Tyr103, and W3 forms a hydrogen bond to the carboxylates of Glu113 and Glu138. On the other hand, W2 forms a hydrogen bond to two other water molecules, but no protein atoms. These waters are involved in an elaborate hydrogen bonding network that is disrupted when toxoflavin binds.

Finally, the structure of the holo TflA−toxoflavin complex shows a metal center having square pyramidal geometry (Figure 4C). Ligands are provided by Nε2 of His60, W3, O5 of toxoflavin, and the carboxylates of Glu113 and Glu138. The vacant coordination site is trans to the carboxylate of Glu113 and corresponds to the position occupied by W2 in the holoenzyme. O5 of toxoflavin is located at the site occupied by W1 in the apo- and holoenzymes and is the only toxoflavin atom that chelates Mn(II). W3 occupies the same position in both the holoenzyme and holo TflA−toxoflavin complex and appears to be neutral on the basis of its distance from Mn(II) of 2.2 Å.

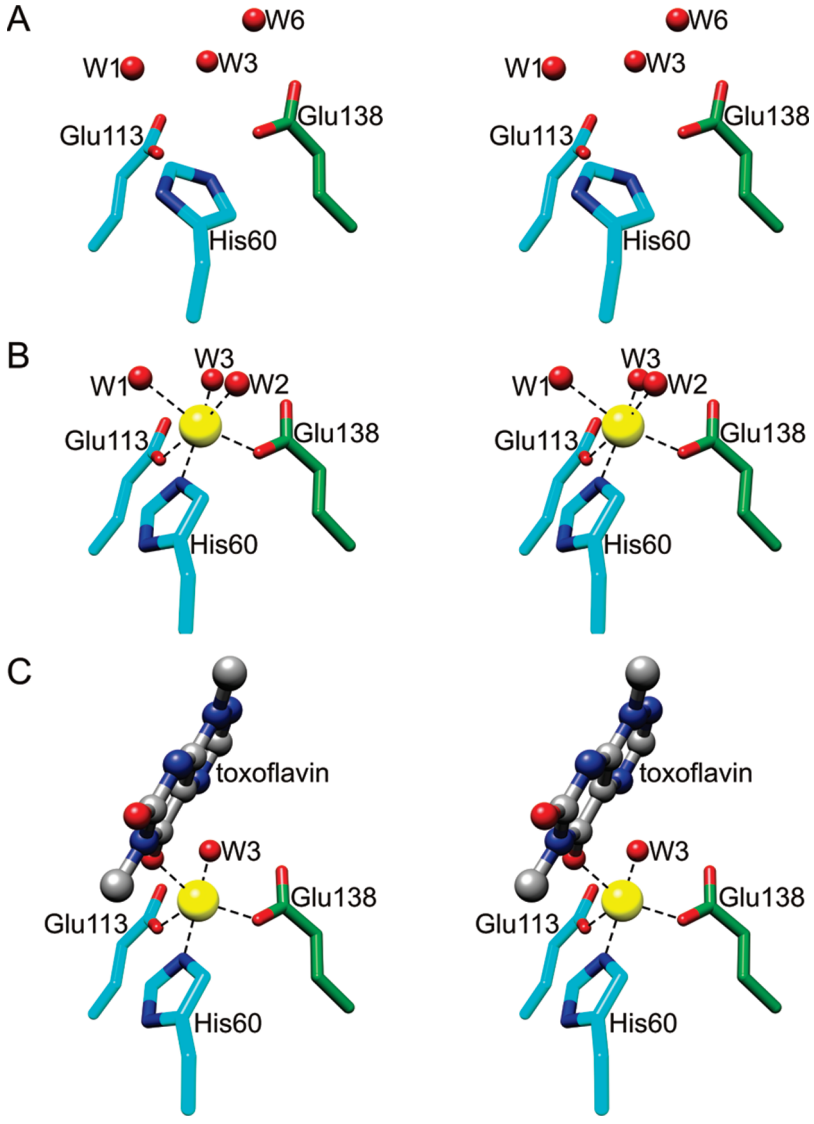

FIGURE 4: TflA metal binding site. (A) Apo TflA. (B) Holo TflA. (C) TflA−toxoflavin−Mn(II) complex. Atoms are color-coded as in Figure 3.

Model of Peroxytoxoflavin Bound to TflA. A model of peroxytoxoflavin in the active site of TflA is shown in Figure 5. Covalent addition of molecular oxygen to C4a of reduced toxoflavin is predicted to result in tetrahedral geometry at this position. Construction of a peroxytoxoflavin−TflA molecular model shows that the tetrahedral geometry can be achieved while maintaining an octahedral coordination sphere. All five of the resulting oxygen−Mn(II)−ligand angles are within 13.0° of the ideal octahedral angles. The resulting O−O−Mn(II) angle is 128.8°, and the separation distance between Mn and the distal peroxy oxygen atom is 2.2 Å. This geometry results in a bent ligand structure near the peroxy moiety. The opposite side of the ligand near C8a is also slightly bent, but its local geometry results in a higher degree of planarity. All of the key interactions observed in the holo TflA−toxoflavin complex are also present in the structure of the putative peroxytoxoflavin intermediate without a significant change in the associated interatomic distances.

Biochemical Analysis of TflA. Initial attempts to reconstitute the in vitro activity of TflA were made by premixing toxoflavin, Mn(II), and DTT, and the reaction was initiated by the addition of TflA. These initial attempts resulted in extremely small amounts of the toxoflavin degradation product being formed. Upon closer inspection, it was determined that prior to TflA addition the addition of DTT caused the characteristic yellow color of toxoflavin to disappear. UV−vis spectroscopic investigations revealed a marked spectral shift when toxoflavin and DTT were mixed in the absence of TflA (Figure 6A). The reaction product was unstable and rapidly reoxidized to toxoflavin in the presence of oxygen (Figure 6A). This is similar to the findings of Latuasan and Berends (*3*) and their investigations with yeast cell free lysate and NADPH. These results led to the hypothesis that the reduced form of toxoflavin was the species bound to and acted upon by TflA. Therefore, all assays were initiated by the addition of DTT rather than enzyme because of the rapidity of the reoxidation of toxoflavin.

Initial studies of TflA activity revealed that a single product was formed as determined via HPLC, and its formation was dependent on TflA, Mn(II), and DTT (Figure 6B). Other reductants, such as NADH and sodium dithionite, also resulted in product formation, although the level of conversion was not as high as that seen with DTT.

Treatment of TflA with EDTA abolished catalytic activity, suggesting that the reaction requires a metal. Addition of metal ions to the apoenzyme resulted in high activity for Mn(II), very low activity for Fe(II), and no activity for Fe(III), Cu(I), Cu(II), Co(II), or Ba(II). The requirement for oxygen was also investigated

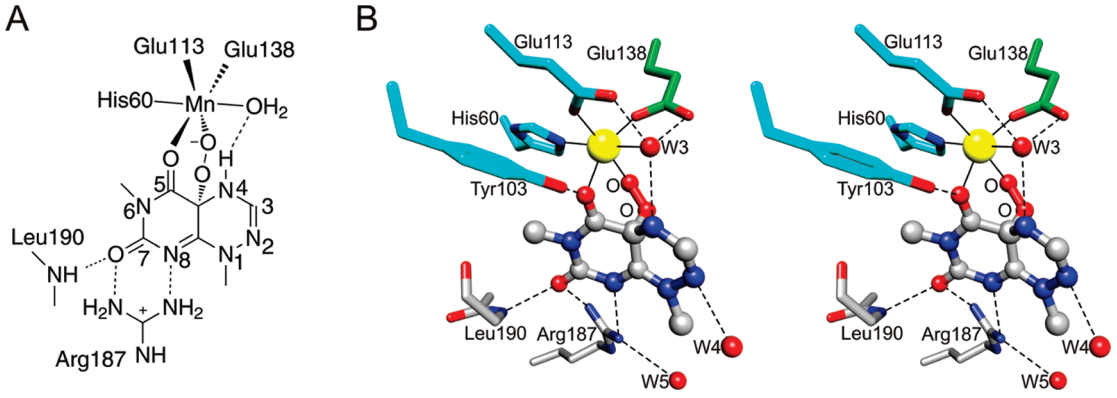

FIGURE 5: Structure of a proposed peroxytoxoflavin intermediate. (A) Schematic of the peroxytoxoflavin intermediate showing key interactions with active site residues. (B) Stereodiagram of the molecular model. Atoms are color-coded as in Figure 3.

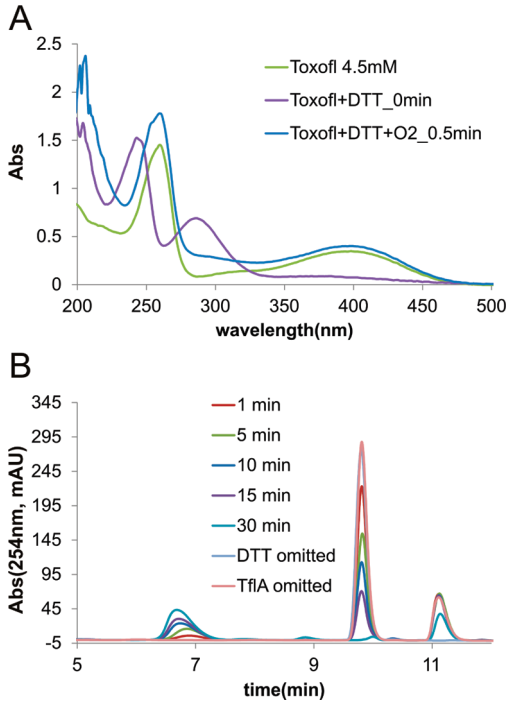

FIGURE 6: In vitro assays. (A) UV−visible spectra of toxoflavin (4.5 mM, green trace); toxoflavin (4.5 mM) and DTT (5 mM), immediately following mixing (purple trace); and toxoflavin (4.5 mM) and DTT (5 mM), following exposure to air for 30 s (blue trace). (B) Time courses for the toxoflavin lyase-catalyzed reaction. The product elutes at 6.7 min, while toxoflavin elutes at 9.9 min. Spectra were recorded on a Nanodrop 2000 using a volume of 1 μL.

because BLAST analysis revealed weak homology to dioxygenases. Assembly of the reaction mixture in an anaerobic environment followed by incubation either anaerobically or aerobically demonstrated that oxygen was essential for product formation. In addition, the presence of hydrogen peroxide did not afford product when DTT was omitted from the reaction mixture (data not shown), suggesting that either the peroxytoxoflavin intermediate is essential for catalysis or the oxidized form of toxoflavin is unable to bind to the active site of TflA.

DISCUSSION

Similarity of TflA to Other Proteins. Alignment of the structure of TflA against structures in the Protein Data Bank (*28*) using the DALI server (*29*) indicates that TflA is structurally homologous to several proteins. Hypothetical proteins 1ZSW and 3OAJ have the highest *Z* scores of 12.1 and 11.5, respectively. The structural alignments include approximately 80% of the TflA residues and show sequence identities with TflA of 11 and 14%, respectively. These two homologues contain two α/β domains that are each composed of an eight-stranded β-sheet with α-helices near the first and last β-strand. Similar to TflA, the two domains are related by pseudo-2-fold symmetry and are constructed from similar $\beta\alpha\beta\beta\beta$ modules. However, only two subdomains of TflA contain complete $\beta\alpha\beta\beta\beta$ modules (M_1 and M_2), whereas these homologues contain four complete $\beta\alpha\beta\beta\beta$ modules. Furthermore, whereas TflA has a metal binding site located between subdomains M_2 and M_3, these homologues have a metal binding site between subdomains M_1 and M_4.

Many of the remaining structural homologues identified by the DALI search are members of the VOC superfamily and have known functions. These homologues include glyoxalases (PDB entries 1FRO and 1FA5) (*30*, *31*), methylmalonyl-CoA epimerases (PDB entry 1JC5) (*32*), fosfomycin resistance proteins (PDB entry 1LQP) (*33*), extradiol (PDB entries 1HAN, 1MPY, 1DHY, and 1F1U) (*34*−*37*) and α-keto acid-dependent dioxygenases (PDB entries 1T47 and 1CJX) (*38*, *39*), and nonenzymatic bleomycin resistance proteins (PDB entry 1BYL) (*40*). These homologues have DALI *Z* scores between 5.0 and 9.0 and display diverse sequences with less than 20% identity compared to TflA. Like TflA, these proteins form structures of two domains, which contain mixed β-sheets built primarily from $\beta\alpha\beta\beta\beta$-like modules. The extradiol- and α-keto acid-dependent dioxygenases form such structures via a single polypeptide chain comprising four tandem $\beta\alpha\beta\beta\beta$-like modules, similar to proteins 1ZSW and 3OAJ. In contrast, the glyoxalases, methylmalonyl-CoA epimerases, and fosfomycin and bleomycin resistance proteins are homodimers with each protomer containing tandem $\beta\alpha\beta\beta\beta$-like modules.

Despite the low sequence identity between TflA and its structural homologues, the primary structure of TflA contains well-defined signature sequences of the $\beta\alpha\beta\beta\beta$ modules of VOC superfamily proteins (*12*). For M_1 and M_3 of structures containing four $\beta\alpha\beta\beta\beta$ modules, the signature sequence is $S_{1,3}$ [$DX_6FXTX_2LG(F,M,L)X_6D$] and occurs near the single α-helix. For modules M_2 and M_4, $S_{2,4}$ [(D,T)PXGX_2(L,V,I)(E,H)] occurs near the $\beta_3\beta_4$ fragment. LG(F,M,L) in $S_{1,3}$ and PXG in $S_{2,4}$ have also been shown to be highly conserved (*12*). The stretch of residues Glu13−Asp35 in M_1 of TflA, specifically ELDRMLAFYTNMLGAQHVHEQAD, is homologous to $S_{1,3}$, with LG being located at the C-terminal end of the α-helix. Furthermore,

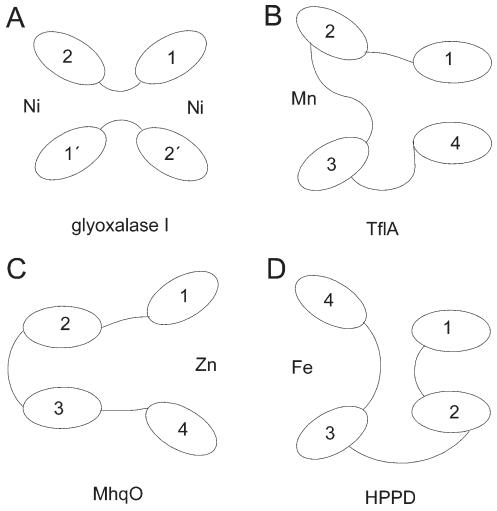

FIGURE 7: Modular arrangements in enzymes containing $\beta\alpha\beta\beta\beta$ folds. (A) Homodimeric family containing modules M_1 and M_2 and two metal binding sites, represented by glyoxalase I (PDB entry 1F9Z). (B) Four-module arrangement in TflA. (C) Four-module arrangement in MhqO (PDB entry 3OAJ). (D) Four-module arrangement in HPPD (PDB entry 1CJX).

DPSGNIIE (106−113), which resides in and between β_3 and β_4 of M_2, is equivalent to $S_{2,4}$. Structurally, LG(F,M,L) acts as a helix termination sequence and PXG a turn sequence. In TflA, the Leu25-Gly26-Ala27 triad terminates the α-helix in M_2. The Asp106-Pro107-Ser108-Gly109 sequence forms a type 1 β-turn. The signature sequences are not found in modules M_3 and M_4.

Domain Structure of TflA. Studies of the evolution of the VOC superfamily suggest that members derive from a homodimeric ancestor in which each monomer contains two modules (*10*−*13*). Each of the two identical metal binding sites of the ancestral enzymes (represented by glyoxalase I, PDB entry 1F9Z) (*31*) utilizes residues from both subdomains through domain swapping (Figure 7A) (*32*). The VOC superfamily members containing four modules likely evolved by gene duplication and fusion of the two-module proteins (*12*). The fused proteins typically have retained only one metal binding site.

Three distinct arrangements of four-module proteins have been observed. One domain of TflA is formed from M_1 and M_4, and a second domain is formed from M_2 and M_3 (Figure 7B). The Mn(II) binding site of TflA is located between modules M_2 and M_3, and there are two interdomain crossovers. *Bacillus subtilis* MhqO (PDB entry 3OAJ), a putative ring-cleaving dioxygenase, shows a modular arrangement similar to that of TflA (Figure 7C); however, the metal binding site is located between modules M_1 and M_4. The VOC superfamily enzymes, represented by 4-hydroxyphenylpyruvate dioxygenase (HPPD) (PDB entry 1CJX) (*39*), displays a different modular arrangement in which M_1 and M_2 form one domain and M_3 and M_4 form another (Figure 7D). The diversity of domain arrangements and metal binding sites suggests multiple evolutionary paths involving gene fusion, domain swapping (*41*), circular permutation (*42*, *43*), and individual amino acid mutations.

Comparison with the 2-His-1-Carboxylate Facial Triad. The 2-His-1-carboxylate facial triad is a common structural motif found in mononuclear non-heme Fe(II) enzymes that activate molecular oxygen (*14*, *44*, *45*). As its name implies, the metal binding protein ligands occupy a face of an octahedral coordination sphere. However, metal chelation by the triad carboxylate

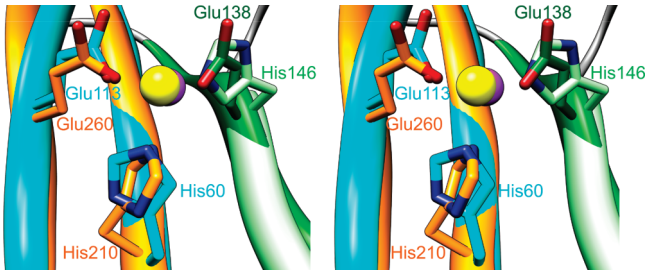

FIGURE 8: Comparison of 1-His-2-carboxylate and 2-His-1-carboxylate facial triads. A stereodiagram is shown for the superimposition of the backbone atoms of the three metal-binding ligands of TflA on the equivalent atoms in DHBD. The yellow sphere represents Mn(II) bound by TflA, and the purple sphere signifies Fe(II) bound by DHBD. Coordinating waters and ligands are not shown. The carbon backbone and ribbon representation of residues in M_2, M_3, and M_4 are colored cyan, green (or light green for DHBD), and orange, respectively.

can be mono- or bidentate depending on the enzyme. Thus, up to three exogenous ligands can bind to the metal center, making the facial triad a versatile motif for mediating a wide range of chemical transformations. Accordingly, the 2-His-1-carboxylate facial triad is found in a variety of enzymes, including the VOC superfamily, extradiol, and α-keto acid-dependent dioxygenases that are structurally homologous to TflA (*46*).

TflA shows a variation of the 2-His-1-carboxylate facial triad. In this case, a histidine residue is replaced with one glutamate residue, resulting in a 1-His-2-carboxylate facial triad that thus far is observed only in TflA. Figure 8 shows the 2-His-1-carboxylate facial triad of Fe(II)-dependent 2,3-dihydroxybiphenyl 1,2-dioxygenase (DHBD) (*34*−*37*) superimposed on the 1-His-2-carboxylate facial triad of Mn(II)-dependent TflA. The metal-binding ligands display similar spatial arrangements but are located in different structural modules. The metal−ligand distances in the two structures are similar; the largest deviation is seen for Glu260 of DHBD, whose metal separation distance is ~0.2 Å shorter than that of Glu113 in TflA. In the absence of substrate, the facial triad of TflA binds to three water molecules with octahedral geometry. In contrast, the facial triad of DHBD binds to two water molecules in a square-pyramidal arrangement.

Mechanistic Implications. TflA is a member of the VOC superfamily and shows structural similarities to dioxygenases. TflA requires oxygen, a reducing agent, and Mn(II), which is chelated by a novel 1-His-2-carboxylate facial triad. These observations suggest that degradation of toxoflavin requires the reduced form of toxoflavin and occurs through a peroxytoxoflavin−TflA intermediate. Modeling studies show that the active site can accommodate such an intermediate while maintaining an energetically feasible geometry (Figure 5).

The reduced form of toxoflavin inferred from the structure may be negatively charged because N4 is likely protonated and N8 deprotonated. On the basis of the chemical structure of toxoflavin and the interaction of toxoflavin with TflA, this putative charge presumably resides partially on O7 and N8 and is stabilized through a salt bridge with the guanidinium group of Arg187 and through the hydrogen bond between O7 and the backbone amide nitrogen of Leu190. The protonation of N4 appears to be stabilized through hydrogen bonding with water W3, which is oriented to accept a hydrogen bond because of the hydrogen bonds it donates to the two metal-binding carboxylates. The predicted negative charge on toxoflavin is expected to

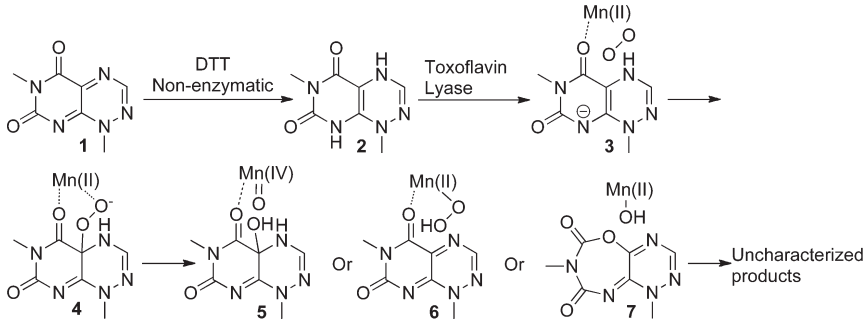

FIGURE 9: Mechanistic proposal for the early steps in the toxoflavin lyase-mediated toxoflavin oxidation.

enhance the reductive activation of O_2 to give the peroxytoxoflavin intermediate.

Dioxygen-activating non-heme Fe(II) enzymes commonly display pentadentate coordination of Fe(II) after substrate or cofactor binding (*46*). Thus, this binding step primes the metal center for coordination by dioxygen. In the extradiol dioxygenases of the VOC superfamily, this is achieved through metal coordination by catecholic hydroxyls on the substrate, one of which is deprotonated (*37*, *47*). In the α-keto acid-dependent enzymes of the VOC superfamily, this is achieved through metal binding by the α-keto acid in a bidentate fashion utilizing the keto and carboxylate oxygens (*48*). Similarly, binding of toxoflavin to Mn(II) in TflA leads to pentadentate coordination with the open site anticipated to be the dioxygen binding site. However, unlike the dioxygenases, only one atom of the substrate (O5 of toxoflavin) chelates Mn(II); the other site is occupied by water W3. In addition, Mn(II) does not appear to be chelated by an anionic group, which is likely related to the neutrality of the combination of Mn(II) and the 1-His-2-carboxylate ligands. Finally, the pentadentate metal center does not involve coordination by vicinal oxygens on the substrate.

Because of the paucity of characteristic NMR features, the product of the TflA-catalyzed reaction has not yet been determined. The structure of the enzyme−toxoflavin complex, however, suggests a mechanism for the early events in toxoflavin oxidation that provides a framework for considering possible reaction products. In this mechanism (Figure 9), toxoflavin is reduced by DTT to give dihydrotoxoflavin. This reduction is nonenzymatic and reversible. We suggest structure **2** for the reduction product by analogy to the structure of dihydroflavin (*49*). This then binds to the enzyme and is oxidized to hydroperoxide **4**. Analogous chemistry is found in the oxidation of dihydroflavin to give the well-characterized flavin hydroperoxide (*49*). We envision three possibilities for the next step. Cleavage of the O−O bond would give **5**, which could then undergo rearrangement of the hydroxytoxoflavin, as previously seen for hydroxyflavin (*50*), and oxidized guanosine (*51*) followed by further oxidation by the Mn(IV) oxo species. Aspects of this chemistry have precedent in the mechanism of the biopterin-dependent phenylalanine hydroxylase (*52*). Alternatively, elimination of hydroperoxide, a reaction frequently seen in the aerobic oxidation of dihydroflavin (*49*), would give **6**, which could undergo further peroxide-mediated oxidation or ring A opening reactions (*53*). The third possibility involves the ring expansion via a Baeyer−Villiger reaction producing **7** and Mn(II)-OH. Product identification is essential for differentiating between these possibilities. This is being pursued using a comprehensive set of ^{13}C- and ^{15}N-labeled toxoflavin isotopologues, which will facilitate unambiguous NMR characterization.

ACKNOWLEDGMENT

We thank the staff of NE-CAT at the Advanced Photon Source and the staff of the Cornell High Energy Synchrotron Source for assistance with data collection, Dr. Cynthia Kinsland for cloning and purifying initial samples of native TflA, and Leslie Kinsland for help in preparing the manuscript.

REFERENCES

1. Levenberg, B., and Linton, S. N. (1966) On the biosynthesis of toxoflavin, an azapteridine antibiotic produced by *Pseudomonas cocovenenans*. *J. Biol. Chem. 241*, 846–852.
2. Lynch, K. H., and Dennis, J. J. (2010) Burkholderia. In Molecular detection of foodborne pathogens (Liu, D., Ed.) pp 331−343, CRC Press, Boca Raton, FL.
3. Latuasan, H. E., and Berends, W. (1961) On the origin of the toxicity of toxoflavin. *Biochim. Biophys. Acta 52*, 502–508.
4. Stern, K. G. (1935) Oxidation-reduction potentials of toxoflavin. *Biochem. J. 29*, 500–508.
5. Goto, K., and Ohata, K. (1956) New bacterial diseases of rice (brown stripe and grain rot). *Nippon Shokubutsu Byori Gakkaiho 21*, 46–47.
6. Jeong, Y., Kim, J., Kim, S., Kang, Y., Nagamatsu, T., and Hwang, I. (2003) Toxoflavin produced by *Burkholderia glumae* causing rice grain rot is responsible for inducing bacterial wilt in many field crops. *Plant Dis. 87*, 890–895.
7. Nandakumar, R., Shahjahan, A. K. M., Yuan, X. L., Dickstein, E. R., Groth, D. E., Clark, C. A., Cartwright, R. D., and Rush, M. C. (2009) *Burkholderia glumae* and *B. gladioli* cause bacterial panicle blight in rice in the southern United States. *Plant Dis. 93*, 896–905.
8. Uematsu, T., Yoshimura, D., Nishiyama, K., Ibaraki, T., and Fujii, H. (1976) Pathogenic bacterium causing seedling rot of rice. *Nippon Shokubutsu Byori Gakkaiho 42*, 464–471.
9. Hwang, I. G., Moon, J. S., and Jwa, N. S. (2009) TflA gene which can degrade toxoflavin and its chemical derivatives and transgenic organisms expressing TflA gene. Organization, W. I. P., Ed.
10. Armstrong, R. N. (2000) Mechanistic diversity in a metalloenzyme superfamily. *Biochemistry 39*, 13625–13632.
11. Babbitt, P. C., and Gerlt, J. A. (1997) Understanding enzyme superfamilies. Chemistry as the fundamental determinant in the evolution of new catalytic activities. *J. Biol. Chem. 272*, 30591–30594.
12. Bergdoll, M., Eltis, L. D., Cameron, A. D., Dumas, P., and Bolin, J. T. (1998) All in the family: Structural and evolutionary relationships among three modular proteins with diverse functions and variable assembly. *Protein Sci. 7*, 1661–1670.
13. Gerlt, J. A., and Babbitt, P. C. (2001) Divergent evolution of enzymatic function: Mechanistically diverse superfamilies and functionally distinct suprafamilies. *Annu. Rev. Biochem. 70*, 209–246.
14. Que, L., Jr. (2000) One motif: Many different reactions. *Nat. Struct. Biol. 7*, 182–184.
15. Laemmli, U. K. (1970) Cleavage of structural proteins during the assembly of the head of bacteriophage T4. *Nature 227*, 680–685.
16. Pace, C. N., Vajdos, F., Fee, L., Grimsley, G., and Gray, T. (1995) How to Measure and Predict the Molar Absorption-Coefficient of a Protein. *Protein Sci. 4*, 2411–2423.
17. Otwinowski, Z., and Minor, W. (1997) Processing of X-ray diffraction data collected in oscillation mode. In Methods in Enzymology (Carter, C. W., Jr., and Sweet, R. M., Eds.) pp 307−326, Academic Press, New York.
18. Schneider, T. R., and Sheldrick, G. M. (2002) Substructure solution with SHELXD. *Acta Crystallogr. D58*, 1772–1779.

19. Sheldrick, G. M. (2008) A short history of SHELX. *Acta Crystallogr. A64*, 112–122.
20. Adams, P. D., Afonine, P. V., Bunkóczi, G., Chen, V. B., Davis, I. W., Echols, N., Headd, J. J., Hung, L.-W., Kapral, G. J., Grosse-Kunstleve, R. W., McCoy, A. J., Moriarty, N. W., Oeffner, R., Read, R. J., Richardson, D. C., Richardson, J. S., Terwilliger, T. C., and Zwart, P. H. (2010) PHENIX: A comprehensive Python-based system for macromolecular structure solution. *Acta Crystallogr. D66*, 213–221.
21. Emsely, P., Lohkamp, B., Scott, W. G., and Cowtan, K. (2010) Features and development of Coot. *Acta Crystallogr. D66*, 486–501.
22. Moriarty, N. W., Grosse-Kunstleve, R. W., and Adams, P. D. (2009) electronic Ligand Builder and Optimization Workbench (eLBOW): A tool for ligand coordinate and restraint generation. *Acta Crystallogr. D65*, 1074–1080.
23. Word, J. M., Lovell, S. C., Richardson, J. S., and Richardson, D. C. (1999) Asparagine and glutamine: Using hydrogen atom contacts in the choice of side-chain amide orientation. *J. Mol. Biol. 285*, 1735–1747.
24. Laskowski, R. A., MacArthur, M. W., Moss, D. S., and Thornton, J. M. (1993) PROCHECK: A program to check the stereochemical quality of protein structures. *J. Appl. Crystallogr. 26*, 283–291.
25. Black, T. H. (1987) An improved, large-scale synthesis of xanthothricin and reumycin. *J. Heterocycl. Chem. 24*, 1373–1375.
26. Goddard, T. D., Huang, C. C., and Ferrin, T. E. (2007) Visualizing density maps with UCSF Chimera. *J. Struct. Biol. 157*, 281–287.
27. Pettersen, E. F., Goddard, T. D., Huang, C. C., Couch, G. S., Greenblatt, D. M., Meng, E. C., and Ferrin, T. E. (2004) UCSF Chimera: A visualization system for exploratory research and analysis. *J. Comput. Chem. 25*, 1605–1612.
28. Berman, H. M., Battistuz, T., Bhat, T. N., Bluhm, W. F., Bourne, P. E., Burkhardt, K., Feng, Z., Gilliland, G. L., Iype, L., Jain, S., Fagan, P., Marvin, J., Padilla, D., Ravichandran, V., Schneider, B., Thanki, N., Weissig, H., Westbrook, J. D., and Zardecki, C. (2002) The Protein Data Bank. *Acta Crystallogr. D58*, 899–907.
29. Holm, L., and Rosenstrom, P. (2010) Dali server: Conservation mapping in 3D. *Nucleic Acids Res. 38* (Suppl.), W545–W549.
30. Cameron, A. D., Olin, B., Ridderstrom, M., Mannervik, B., and Jones, T. A. (1997) Crystal structure of human glyoxalase I: Evidence for gene duplication and 3D domain swapping. *EMBO J. 16*, 3386–3395.
31. He, M. M., Clugston, S. L., Honek, J. F., and Matthews, B. W. (2000) Determination of the structure of *Escherichia coli* glyoxalase I suggests a structural basis for differential metal activation. *Biochemistry 39*, 8719–8727.
32. McCarthy, A. A., Baker, H. M., Shewry, S. C., Patchett, M. L., and Baker, E. N. (2001) Crystal structure of methylmalonyl-coenzyme A epimerase from *P. shermanii*: A novel enzymatic function on an ancient metal binding scaffold. *Structure 9*, 637–646.
33. Rife, C. L., Pharris, R. E., Newcomer, M. E., and Armstrong, R. N. (2002) Crystal structure of a genomically encoded fosfomycin resistance protein (FosA) at 1.19 Å resolution by MAD phasing off the L-III edge of Tl^{+}. *J. Am. Chem. Soc. 124*, 11001–11003.
34. Han, S., Eltis, L. D., Timmis, K. N., Muchmore, S. W., and Bolin, J. T. (1995) Crystal structure of the biphenyl-cleaving extradiol dioxygenase from a PCB-degrading pseudomonad. *Science 270*, 976–980.
35. Kita, A., Kita, S., Fujisawa, I., Inaka, K., Ishida, T., Horiike, K., Nozaki, M., and Miki, K. (1999) An archetypical extradiol-cleaving catecholic dioxygenase: The crystal structure of catechol 2,3-dioxygenase (metapyrocatechase) from *Pseudomonas putida* mt-2. *Structure 7*, 25–34.
36. Senda, T., Sugiyama, K., Narita, H., Yamamoto, T., Kimbara, K., Fukuda, M., Sato, M., Yano, K., and Mitsui, Y. (1996) Three-dimensional structures of free form and two substrate complexes of an extradiol ring-cleavage type dioxygenase, the BphC enzyme from *Pseudomonas* sp. strain KKS102. *J. Mol. Biol. 255*, 735–752.
37. Vetting, M. W., Wackett, L. P., Que, L., Jr., Lipscomb, J. D., and Ohlendorf, D. H. (2004) Crystallographic comparison of manganese- and iron-dependent homoprotocatechuate 2,3-dioxygenases. *J. Bacteriol. 186*, 1945–1958.
38. Brownlee, J. M., Johnson-Winters, K., Harrison, D. H., and Moran, G. R. (2004) Structure of the ferrous form of (4-hydroxyphenyl)-pyruvate dioxygenase from *Streptomyces avermitilis* in complex with the therapeutic herbicide, NTBC. *Biochemistry 43*, 6370–6377.
39. Serre, L., Sailland, A., Sy, D., Boudec, P., Rolland, A., Pebay-Peyroula, E., and Cohen-Addad, C. (1999) Crystal structure of *Pseudomonas fluorescens* 4-hydroxyphenylpyruvate dioxygenase: An enzyme involved in the tyrosine degradation pathway. *Structure 7*, 977–988.
40. Dumas, P., Bergdoll, M., Cagnon, C., and Masson, J. M. (1994) Crystal structure and site-directed mutagenesis of a bleomycin resistance protein and their significance for drug sequestering. *EMBO J. 13*, 2483–2492.
41. Saint-Jean, A. P., Phillips, K. R., Creighton, D. J., and Stone, M. J. (1998) Active monomeric and dimeric forms of *Pseudomonas putida* glyoxalase I: Evidence for 3D domain swapping. *Biochemistry 37*, 10345–10353.
42. Cunningham, B. A., Hemperly, J. J., Hopp, T. P., and Edelman, G. M. (1979) Favin versus concanavalin A: Circularly permuted amino acid sequences. *Proc. Natl. Acad. Sci. U.S.A. 76*, 3218–3222.
43. Lindqvist, Y., and Schneider, G. (1997) Circular permutations of natural protein sequences: Structural evidence. *Curr. Opin. Struct. Biol. 7*, 422–427.
44. Gerlt, J. A., and Babbitt, P. C. (1998) Mechanistically diverse enzyme superfamilies: The importance of chemistry in the evolution of catalysis. *Curr. Opin. Chem. Biol. 2*, 607–612.
45. Laughlin, L. T., Bernat, B. A., and Armstrong, R. N. (1998) Mechanistic imperative for the evolution of a metalloglutathione transferase of the vicinal oxygen chelate superfamily. *Chem.-Biol. Interact. 111−112*, 41–50.
46. Koehntop, K. D., Emerson, J. P., and Que, L., Jr. (2005) The 2-His-1-carboxylate facial triad: A versatile platform for dioxygen activation by mononuclear non-heme iron(II) enzymes. *J. Biol. Inorg. Chem. 10*, 87–93.
47. Vaillancourt, F. H., Bolin, J. T., and Eltis, L. D. (2006) The ins and outs of ring-cleaving dioxygenases. *Crit. Rev. Biochem. Mol. Biol. 41*, 241–267.
48. He, P., and Moran, G. R. (2009) We two alone will sing: The two-substrate α-keto acid-dependent oxygenases. *Curr. Opin. Chem. Biol. 13*, 443–450.
49. Fagan, R. L., and Palfey, B. A. (2010) Flavin-Dependent Enzymes. In Comprehensive Natural Products II (Lew, M., and Hung-Wen, L., Eds.) pp 37−113, Elsevier, Oxford, U.K.
50. Iwata, M., Bruice, T. C., Carrell, H. L., and Glusker, J. P. (1980) Reactions of 4a-peroxides and 4a-pseudobases of N^{10}- and N^{5}-phenethylflavins. *J. Am. Chem. Soc. 102*, 5036–5044.
51. Ye, Y., Muller, J. G., Luo, W., Mayne, C. L., Shallop, A. J., Jones, R. A., and Burrows, C. J. (2003) Formation of ^{13}C-, ^{15}N-, and ^{18}O-Labeled Guanidinohydantoin from Guanosine Oxidation with Singlet Oxygen. Implications for Structure and Mechanism. *J. Am. Chem. Soc. 125*, 13926–13927.
52. Bassan, A., Blomberg, M. R. A., and Siegbahn, P. E. M. (2003) Mechanism of dioxygen cleavage in tetrahydrobiopterin-dependent amino acid hydroxylases. *Chem.—Eur. J. 9*, 106–115.
53. Mukherjee, T., Zhang, Y., Abdelwahed, S., Ealick, S. E., and Begley, T. P. (2010) Catalysis of a Flavoenzyme-Mediated Amide Hydrolysis. *J. Am. Chem. Soc. 132*, 1550–1551.
54. Kabsch, W., and Sander, C. (1983) Dictionary of protein secondary structure: Pattern recognition of hydrogen-bonded and geometrical features. *Biopolymers 22*, 2577–2637.